PROPELLER/NACELLE WHIRL FLUTTER ADDITION TO MSC/NASTRAN

by

William P. Rodden and Ted L. Rose
The MacNeal-Schwendler Corporation

ABSTRACT

A preprocessor has been developed to include propeller/nacelle aerodynamic and gyroscopic forces in MSC/NASTRAN flutter analysis with SOL 75. The propeller is assumed to be rigid. The effects of wing downwash on the propeller forces are also included. The equations of motion are presented along with two example problems. The first example is a simple two degree of freedom propeller and correlations with wind tunnel data are shown. The second example is the cantilevered BAH wing with a nacelle, propeller and rotor added. The whirl flutter speed is shown along with the effects of the propeller/nacelle on the wing flutter and divergence characteristics. The effects of the wing downwash are also shown. The inclusion of propeller wake effects on the wing loads by using correction factors is discussed.

INTRODUCTION

This paper summarizes the theoretical development and application of a preprocessor for MSC/NASTRAN to add propeller/nacelle aerodynamic and gyroscopic forces for flutter analysis via SOL 75. The propeller is assumed to be rigid. The effects of wing downwash on the propeller aerodynamic forces are also considered. Two examples illustrate the new capability. The first example is an isolated spring-mounted propeller that was tested in a wind tunnel for aerodynamic stability derivatives and flutter speeds, and it illustrates some experimental correlation; it also illustrates certain dummy cards for a wing that are required by SOL 75 when only an isolated propeller/nacelle system is considered. The second example is a propeller/nacelle added to the restrained BAH wing. It illustrates the addition of a nacelle to the wing, the propeller/rotor data for the preprocessor, and the optional effects of the flow field forward of the wing. A discussion of wing/body correction factors to account for propeller slipstream effects is also presented.

NOMENCLATURE

A	=	blade aspect ratio, specified or calculated from Equation 29; also, downwash factor in aerodynamic wing/body theory
A_{Iw}, A_{II}, A_{Is}	=	downwash factors on interference elements from wing boxes, interference elements, and slender body elements
a_0	=	blade airfoil two-dimensional incompressible lift curve slope
a_M	=	blade airfoil two-dimensional transonic lift curve slope

C_m = propeller pitching moment coefficient, positive wing leading edge up

C_n = propeller yawing moment coefficient, positive nose right

C_w = wing box doublet strength

C_y = propeller side force coefficient, positive starboard

C_z = propeller lift coefficient, positive downward

c = local blade chord; also, equivalent viscous structural damping

c_r = reference blade chord

D = propeller diameter

D_{jk} = element of substantial derivative matrix

F = force on propeller

f = cyclic frequency

$F(k)$ = real part of Theodorsen lag function

$G(k)$ = imaginary part of Theodorsen lag function

G_{ka} = element of aerodynamic/structure interpolation matrix

g = acceleration of gravity; also, structural damping coefficient

I_i = in-phase blade integral

I_p = propeller polar moment of inertia

I_r = rotor polar moment of inertia

I_x = effective propeller/rotor polar moment of inertia

I_y = propeller moment of inertia in pitch and in yaw

J = advance ratio, $J = \pi V/\Omega R$

J_i = out-of-phase (lag) blade integral

k = reduced frequency of blade section, $k = c/2R\sqrt{\mu^2 + \eta^2}$

ℓ_0 = distance between pivot and hub in Reference 5

M = pitching moment on propeller; also, Mach number

N = yawing moment on propeller

N_b = number of propeller blades

N_r = gear ratio, N_r is ratio of rotor rotational speed to that of propeller

n = propeller cyclic rotational speed, rev/s

P_1, P_2 = partitioning matrices

Q_{jh} = element of generalized force matrix for motion

q = pitch rate

$\bar{q}$ = freestream dynamic pressure

R = propeller radius

$R\ell( )$ = real part of ( )

r = radial coordinate of propeller; also, yaw rate

S = propeller disc area

S_s = slipstream cross section area

T = propeller thrust

V = freestream velocity

V_s = slipstream velocity

v = sidewash induced by lifting components

W_{kk} = aerodynamic correction factors to account for propeller slipstream effects

w = downwash induced by lifting components

w_s = width of propeller slipstream

x,y,z = Cartesian coordinate system: NACA stability axis system for propeller, MSC/NASTRAN aerodynamic system for lifting surfaces

Δy = width of wing region behind propeller for slipstream correction factors

$\beta_{0.75R}$ = blade angle at 3/4-radius reference station

η = dimensionless radius, $\eta = r/R$

θ = pitch angle

ψ = yaw angle

μ = advance ratio, $\mu = J/\pi = V/\Omega R$

μ_l, μ_s = doublet strengths of interference elements and slender body elements

ρ = atmospheric density

ϕ_{a_j} = element of i^{th} aerodynamic mode shape matrix

Ω = propeller angular rotational speed, rad/s

ω = vibration frequency, rad/s

$\dot{(\,)}$ = time derivative

Subscripts

θ = refers to pitch; also, partial differentiation with respect to θ, i.e., $\partial/\partial\theta$

ψ = refers to yaw; also, partial differentiation with respect to ψ, i.e., $\partial/\partial\psi$

q = partial differentiation with respect to dimensionless pitch rate, i.e., $\partial/\partial(qD/2V)$

r = partial differentiation with respect to dimensionless yaw rate, i.e., $\partial/\partial(rD/2V)$

THEORETICAL BACKGROUND

A brief bibliography on propeller/nacelle whirl flutter is provided by References 1 - 11. The aerodynamic coefficients for the loads on the propeller hub are given here in the notation (with variations) of Ribner (Reference 12). The right-hand coordinate system is that of Reed and Bland (Reference 1) and is shown in Figure 1. The effects of interference can be included by subtracting the wing/body induced downwash angle w/V from the effective static downwash angle $\theta + \dot{z}/V$, and by adding the induced sidewash angle v/V to the effective static sidewash angle $\psi - \dot{y}/V$ as indicated in Figures 2(a) and (b). The aerodynamic derivatives are defined by the following expressions for propeller forces and moments.

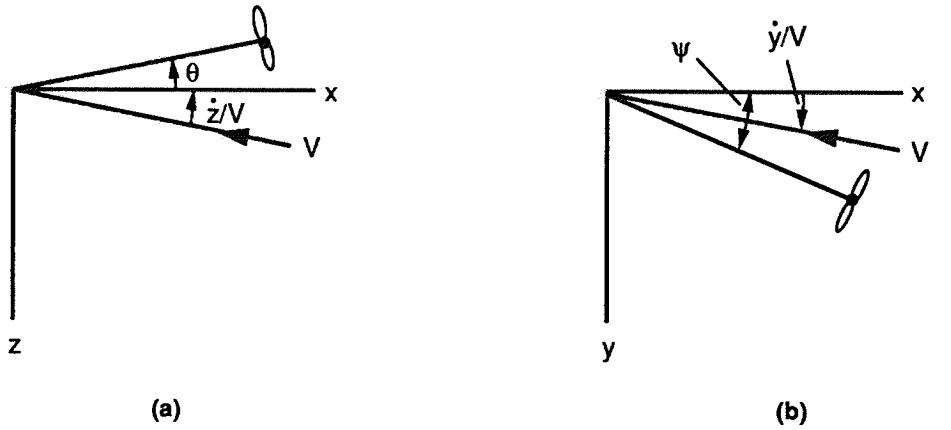

Figure 2. Effective Angles of Attack in Pitch (a) and in Yaw (b).

$$F_z = \bar{q}S \left[C_{z_\theta}(\theta + \dot{z}/V - w/V) + C_{z_\psi}(\psi - \dot{y}/V + v/V) + C_{z_q}(\dot{\theta}D/2V) + C_{z_r}(\dot{\psi}D/2V) \right] \quad (1)$$

$$M = \bar{q}SD \left[C_{m_\theta}(\theta + \dot{z}/V - w/V) + C_{m_\psi}(\psi - \dot{y}/V + v/V) + C_{m_q}(\dot{\theta}D/2V) + C_{m_r}(\dot{\psi}D/2V) \right] \quad (2)$$

$$F_y = \bar{q}S \left[C_{y_\theta}(\theta + \dot{z}/V - w/V) + C_{y_\psi}(\psi - \dot{y}/V + v/V) + C_{y_q}(\dot{\theta}D/2V) + C_{y_r}(\dot{\psi}D/2V) \right] \quad (3)$$

$$N = \bar{q}SD \left[C_{n_\theta}(\theta + \dot{z}/V - w/V) + C_{n_\psi}(\psi - \dot{y}/V + v/V) + C_{n_q}(\dot{\theta}D/2V) + C_{n_r}(\dot{\psi}D/2V) \right] \quad (4)$$

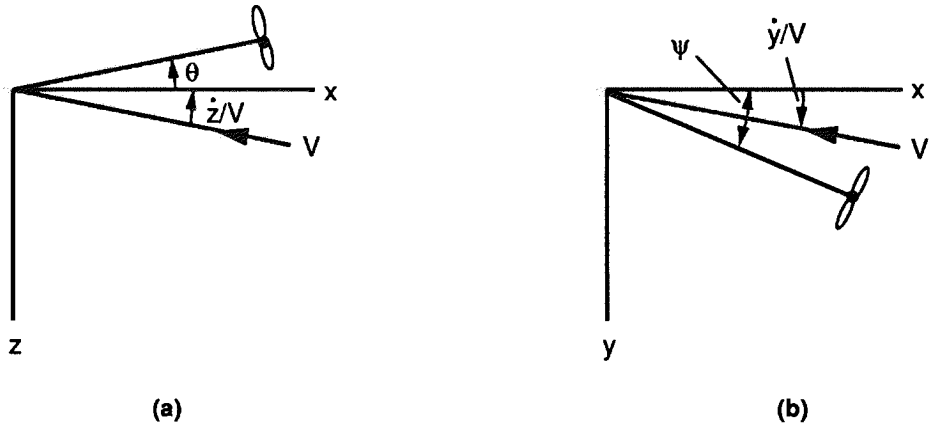

Figure 2. Effective Angles of Attack in Pitch (a) and in Yaw (b).

$$F_z = \bar{q}S \left[C_{z_\theta}\left(\theta + \dot{z}/V - w/V\right) + C_{z_\psi}\left(\psi - \dot{y}/V + v/V\right) + C_{z_q}\left(\dot{\theta}D/2V\right) + C_{z_r}\left(\dot{\psi}D/2V\right) \right] \quad (1)$$

$$M = \bar{q}SD \left[C_{m_\theta}\left(\theta + \dot{z}/V - w/V\right) + C_{m_\psi}\left(\psi - \dot{y}/V + v/V\right) + C_{m_q}\left(\dot{\theta}D/2V\right) + C_{m_r}\left(\dot{\psi}D/2V\right) \right] \quad (2)$$

$$F_y = \bar{q}S \left[C_{y_\theta}\left(\theta + \dot{z}/V - w/V\right) + C_{y_\psi}\left(\psi - \dot{y}/V + v/V\right) + C_{y_q}\left(\dot{\theta}D/2V\right) + C_{y_r}\left(\dot{\psi}D/2V\right) \right] \quad (3)$$

$$N = \bar{q}SD \left[C_{n_\theta}\left(\theta + \dot{z}/V - w/V\right) + C_{n_\psi}\left(\psi - \dot{y}/V + v/V\right) + C_{n_q}\left(\dot{\theta}D/2V\right) + C_{n_r}\left(\dot{\psi}D/2V\right) \right] \quad (4)$$

where S is the propeller disc area

$$S = \pi D^2/4 \tag{5}$$

and the aerodynamic coefficients are given in terms of the blade integrals I_i and J_i.

$$C_{z_\theta} = -(4\Omega c_r/V)\, I_1 \tag{6}$$

$$C_{m_\theta} = -(2\Omega c_r/V)\, J_2 \tag{7}$$

$$C_{y_\theta} = -(4\Omega c_r/V)\, J_1 \tag{8}$$

$$C_{n_\theta} = -(2\Omega c_r/V)\, I_2 \tag{9}$$

$$C_{z_q} = (4\Omega c_r/V)\, J_2 \tag{10}$$

$$C_{m_q} = -(2\Omega c_r/V)\, I_3 \tag{11}$$

$$C_{y_q} = -(4\Omega c_r/V)\, I_2 \tag{12}$$

$$C_{n_q} = -(2\Omega c_r/V)\, J_3 \tag{13}$$

and, by symmetry (see Reference 1),

$$C_{z_\psi} = C_{y_\theta} \tag{14}$$

$$C_{m_\psi} = -C_{n_\theta} \tag{15}$$

$$C_{y_\psi} = -C_{z_\theta} \tag{16}$$

$$C_{n_\psi} = C_{m_\theta} \tag{17}$$

$$C_{z_r} = C_{y_q} \tag{18}$$

$$C_{m_r} = -C_{n_q} \tag{19}$$

$$C_{y_r} = -C_{z_q} \tag{20}$$

$$C_{n_r} = C_{m_q} \tag{21}$$

The blade integrals are (see Reference 2)

$$I_1 = \left(\frac{N_b}{4}\right)\left(\frac{a_0}{2\pi}\right)\frac{\mu^2 A}{c_r}\int_{\eta_0}^{1}\frac{c(\eta)\ F(k)}{\sqrt{\mu^2+\eta^2}\left[2+A\sqrt{1-M^2(1+\eta^2/\mu^2)}\right]}\,d\eta \tag{22}$$

$$J_1 = \left(\frac{N_b}{4}\right)\left(\frac{a_0}{2\pi}\right)\frac{\mu^2 A}{c_r}\int_{\eta_0}^{1}\frac{c(\eta)\ G(k)}{\sqrt{\mu^2+\eta^2}\left[2+A\sqrt{1-M^2(1+\eta^2/\mu^2)}\right]}\,d\eta \tag{23}$$

$$I_2 = \left(\frac{N_b}{4}\right)\left(\frac{a_0}{2\pi}\right)\frac{\mu A}{c_r}\int_{\eta_0}^{1}\frac{\eta^2\ c(\eta)\ F(k)}{\sqrt{\mu^2+\eta^2}\left[2+A\sqrt{1-M^2(1+\eta^2/\mu^2)}\right]}\,d\eta \tag{24}$$

$$J_2 = \left(\frac{N_b}{4}\right)\left(\frac{a_0}{2\pi}\right)\frac{\mu A}{c_r}\int_{\eta_0}^{1}\frac{\eta^2\ c(\eta)\ G(k)}{\sqrt{\mu^2+\eta^2}\left[2+A\sqrt{1-M^2(1+\eta^2/\mu^2)}\right]}\,d\eta \tag{25}$$

$$I_3 = \left(\frac{N_b}{4}\right)\left(\frac{a_0}{2\pi}\right)\frac{A}{c_r}\int_{\eta_0}^{1}\frac{\eta^4\ c(\eta)\ F(k)}{\sqrt{\mu^2+\eta^2}\left[2+A\sqrt{1-M^2(1+\eta^2/\mu^2)}\right]}\,d\eta \tag{26}$$

$$J_3 = \left(\frac{N_b}{4}\right)\left(\frac{a_0}{2\pi}\right)\frac{A}{c_r}\int_{\eta_0}^{1}\frac{\eta^4\ c(\eta)\ G(k)}{\sqrt{\mu^2+\eta^2}\left[2+A\sqrt{1-M^2(1-\eta^2/\mu^2)}\right]}\,d\eta \tag{27}$$

in which the reduced frequency k is

$$k = c/2R\sqrt{\mu^2+\eta^2} \tag{28}$$

and the blade aspect ratio A is

$$A = \frac{D}{c_r}\,\frac{(1-\eta_0)^2}{\int_{\eta_0}^{1}(c/c_r)\,d\eta} \tag{29}$$

The blade integrals above include the Mach number and aspect ratio corrections suggested in Reference 2, as well as the lift lag due to nonsteady flow, also suggested in Reference 2. Three modifications to Reference 2 are shown above. The first is the lower limit of the integration is taken as η_0, the inside dimensionless radius of the thrusting region of the blade. The second is that the coefficient $(a_0/2\pi)$ is introduced to account for the blade airfoil incompressible lift curve slope differing from 2π as was assumed in Reference 2. Finally, the factor $(N_b/4)$ is introduced to account for the number of blades being different from 4 as was assumed in Reference 2.

In order to avoid problems with the Mach number correction with a supersonic tip in an overspeed condition, a cut-off-value of compressible lift curve slope, a_m, is enforced: wherever $M^2(1 + \eta^2/\mu^2) > 1 - (a_0/a_M)^2$, the value of $M^2(1 + \eta^2/\mu^2)$ is set equal to $1 - (a_0/a_M)^2$.

Although expressions have been given for all 16 propeller coefficients, four of them are usually taken as zero because of their smallness and the lack of experimental correlation for their calculated values. Therefore the coefficients $C_{m_r} = -C_{n_q}$ and $C_{y_r} = -C_{z_q}$ are set to zero.

The induced flow angles may be obtained from the lifting solution and the appropriate partitions of the interference aerodynamic influence coefficients, shown in Equation (4) of Section 2.3.2 of the MSC/NASTRAN Handbook for Aeroelastic Analysis. That equation is reduced as follows to obtain the flow angles and is written as

$$\{w/V, v/V\} = R\ell\,[A_{lw}\ 0\ A_{ls}] \begin{Bmatrix} C_w \\ \mu_l \\ \mu_s \end{Bmatrix} \tag{30}$$

where the downwash angle is obtained from the z-body representation, and both downwash and sidewash angles are obtained from zy-bodies, and only the rows of the A_{ij} for the propeller hub are used. Only the real parts ($R\ell$) of the complex downwashes are considered in Equation (30) to be consistent with the numerous other approximations in the quasi-steady propeller theory, i.e., any aerodynamic damping due to interference is neglected.

The solution for the loads in a mode $\{\phi_{a_i}\}$ is given by

$$\begin{Bmatrix} C_w \\ \mu_l \\ \mu_s \end{Bmatrix} = [A]^{-1}\,[D_{jk}]\,[G_{ka}]\,\{\phi_{a_i}\} \tag{31}$$

and for all of the modes is

$$\begin{bmatrix} C_w \\ \mu_l \\ \mu_s \end{bmatrix} = [Q_{jh}] \tag{32}$$

The MSC/NASTRAN implementation requires a DMAP ALTER to obtain the downwash angles for each mode via

$$[w/V, v/V] = R\ell\,[P_1]\,[A_{lw}\ A_{ll}\ A_{lp}]\,[P_2]\,[Q_{jh}] \tag{33}$$

where $[P_1]$ is a user generated (DMI) partitioning matrix to select the hub vertical and side degrees of freedom and $[P_2]$ is another user generated partitioning matrix to null out $[A_{ll}]$. The downwash and sidewash angles are then multiplied by the appropriate aerodynamic coefficients and dimensional factors and entered into the propeller/wing partition of the stiffness matrix.

No interference of the propeller on the wing is considered here, but the effect of the slipstream on the wing can be accounted for on the aerodynamic boxes in the propeller wake by correction factors to the box areas. The correction factors are discussed at the end of this paper.

The gyroscopic moments are necessary to complete the equations for propeller/rotor effects.

$$M = I_x \Omega \dot{\psi} \tag{34}$$

$$N = -I_x \Omega \dot{\theta} \tag{35}$$

where

$$I_x = I_p + N_r I_r \tag{36}$$

in which I_p is the polar moment of inertia of the propeller, I_r is the polar moment of inertia of the rotor, and N_r is the propeller/rotor gear ratio (the ratio of rotor rotational speed to that of the propeller).

EXAMPLES

NASA TN D-1807 (Reference 5)

A small-scale four-bladed propeller was tested at low speed in the NASA Langley Research Center transonic dynamics tunnel. The model consisted of an isolated, rigid system of the propeller and a simulated power plant mounted with flexibility in pitch and yaw on a rigid sting. Flutter speeds were measured for a range of propeller blade angles, restraint stiffnesses and dampings with a windmilling propeller. Measurements of the propeller aerodynamic stability derivatives were also made by using a simple balance.

The propeller aerodynamic stability derivatives were reported in Figure 10 of Reference 5 as functions of the reference blade angle $\beta_{0.75R}$. Five derivatives were reported: C_{Z_θ}, C_{m_θ}, C_{m_q}, C_{Z_ψ}, and C_{m_ψ}. To obtain the derivatives in the MSC/NASTRAN preprocessor requires input of the forward (V) and rotational (Ω) velocities of the propeller. The reference blade angle for the windmilling propeller is a function of the advance ratio that is related to V and Ω. Two advance ratios are used in the literature, $J = \pi V/\Omega R$ and $\mu = J/\pi = V/\Omega R = V\pi\mu D$, and $\beta_{0.75R}$ is shown as a function of J in Figure 4 of Reference 5. Assuming a typical propeller rotational speed of 1800 RPM, the data from Figure 4 of Reference 5 lead to the results in Table 1. Note that the RPM/velocity combinations used in measuring the aerodynamic coefficients were not reported, so the assumption of 1800 RPM, and the velocities in Table 1 are necessary to calculate the coefficients but do not introduce significant errors because the measurements were made at low Mach numbers.

Table 1. Flight Condition Data for the Aerodynamic Coefficients of NASA TN D-1807.

$\beta_{0.75R}$ (deg)	J	μ	V(ft/s)
25	1.25	0.3979	63.28
35	1.80	0.5730	91.13
46	2.65	0.8435	134.16
52	3.32	1.0568	168.08
58	4.20	1.3369	212.64

The aerodynamic coefficients are calculated with the following additional input parameters: radius R = 0.8438 ft. = 10.1256 in., diameter D = 20.2512 in., reference chord c_r = 4.3752 in., aspect ratio A = 3.47, lift curve slope $a_0 = 2\pi$, maximum transonic lift curve slope $a_M = 4\pi$, and a speed of sound 1116 ft/s. The propeller blade integrals are evaluated from the data in Table 2 derived from Figure 4 of Reference 5.

Table 2. Blade Geometry from NASA TN D-1807.

η	c/c_r	c(in.)	r(in.)
η_0 = 0.17	0.25	0.8750	1.7214
0.20	0.33	1.4438	2.0251
0.21	0.40	1.7501	2.1264
0.22	0.50	2.1876	2.2276
0.23	0.70	3.0626	2.3289
0.24	0.80	3.5002	2.4301
0.25	0.90	3.9377	2.5314
0.27	1.00	4.3752	2.7339
1.00	1.00	4.3752	10.1256

The five computed coefficients are tabulated in Table 3 and are compared with the experimental data in Figure 3. It was expected that the present results would have agreed with those from Reference 2 more closely. However, the agreement with experiment appears reasonable, and the present implementation contains sufficient parameters for tuning the theory to match available propeller data: the incompressible airfoil lift curve slope a_0 can be less than 2π, the high speed lift curve slope a_M can be adjusted to a suitable transonic value, the blade aspect ratio A can be calculated or input, and the inboard limit in the blade integrals η_0 can be moved outboard. Furthermore, the blade chords near the tip can be reduced to account for load reduction near the tip, although the aspect ratio correction is already intended to account for this effect.

Table 3. Calculated Aerodynamic Coefficients for the Propeller of NASA TN D-1807 (Assuming A = 3.47).

$\beta_{0.75R}$	C_{Z_θ}	C_{m_θ}	C_{m_q}	C_{Z_ψ}	C_{m_ψ}
25	-0.331	0.0400	-0.2160	0.0877	0.1506
35	-0.418	0.0362	-0.1391	0.1106	0.1373
46	-0.512	0.0304	-0.0833	0.1320	0.1188
52	-0.566	0.0264	-0.0603	0.1408	0.1067
58	-0.619	0.0221	-0.0422	0.1461	0.0937

The flutter analysis is done to correlate with the first data point in Table II(a) of Reference 5, i.e., with the forward support at $\ell_0/R = 0.346$, blade angle $\beta_{0.75R} = 35°$, pitch frequency $f_\theta = 9.20$ Hz, yaw frequency $f_\psi = 9.12$ Hz, structural dampings in pitch $g_\theta = 0.0060$ and yaw $g_\psi = 0.0090$, air density $\rho = 0.00211$ slugs/cu. ft., and a rotational speed of n = 38.4 revs/s = 2304 RPM.

The preprocessor requires the number of blades $N_b = 4$, the geometry in Table 2, the blade aspect ratio A = 3.47 (which is calculated by Equation (29) if not input), the polar moment of inertia $I_x = 0.00858$ slug-ft^2 = 0.10296 lb-in-s^2, a reference chord $c_r = 4.375$ in., the blade airfoil lift curve slope a_0 = blank or 0 (which gives the default value of 2π), and the maximum transonic lift curve slope a_M = blank or 0 (which gives the default value of 4π). The test air density $\rho = 0.00211$ slug/cu. ft. = 1.0176E-07 lb-s^2/in^4, the velocity, and the speed of sound of 1116 fps are input for each case.

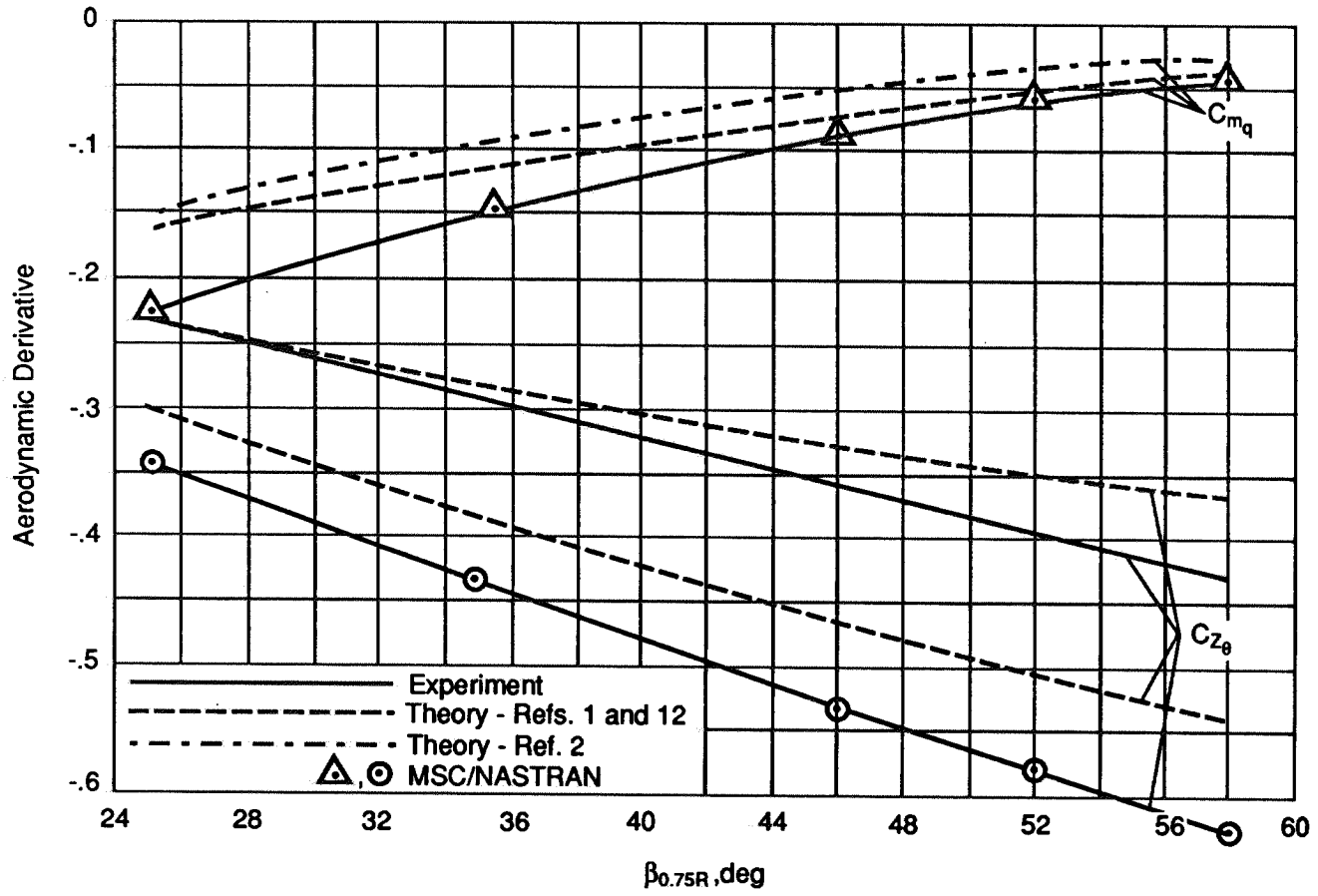

(a) C_{Z_θ} and C_{m_q}.

Figure 3. Comparison of Experimental and Theoretical Aerodynamic Derivatives for the Propeller of NASA TN D-1807.

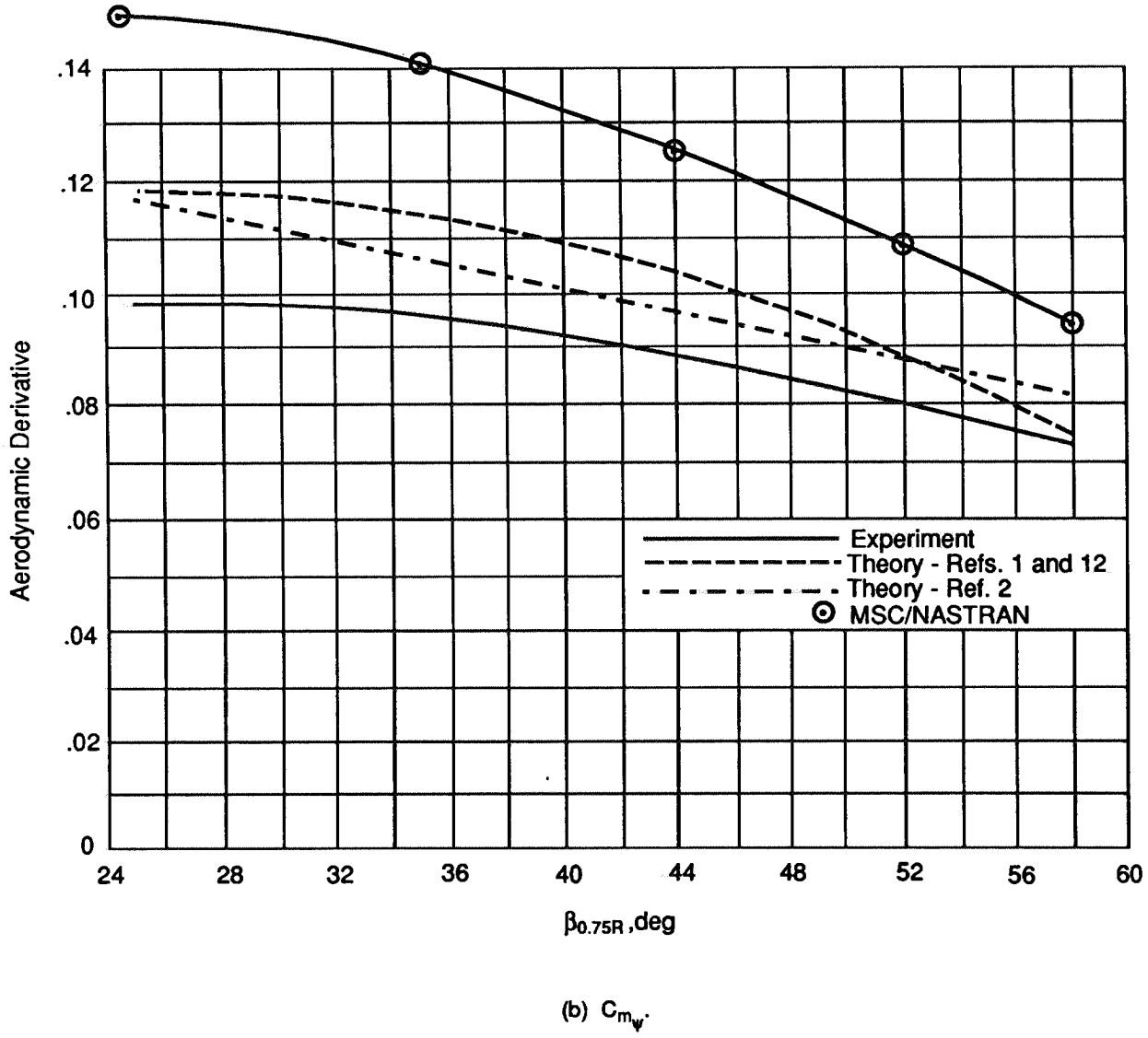

(b) C_{m_ψ}.

Figure 3. Comparison of Experimental and Theoretical Aerodynamic Derivatives for the Propeller of NASA TN D-1807. (Cont.)

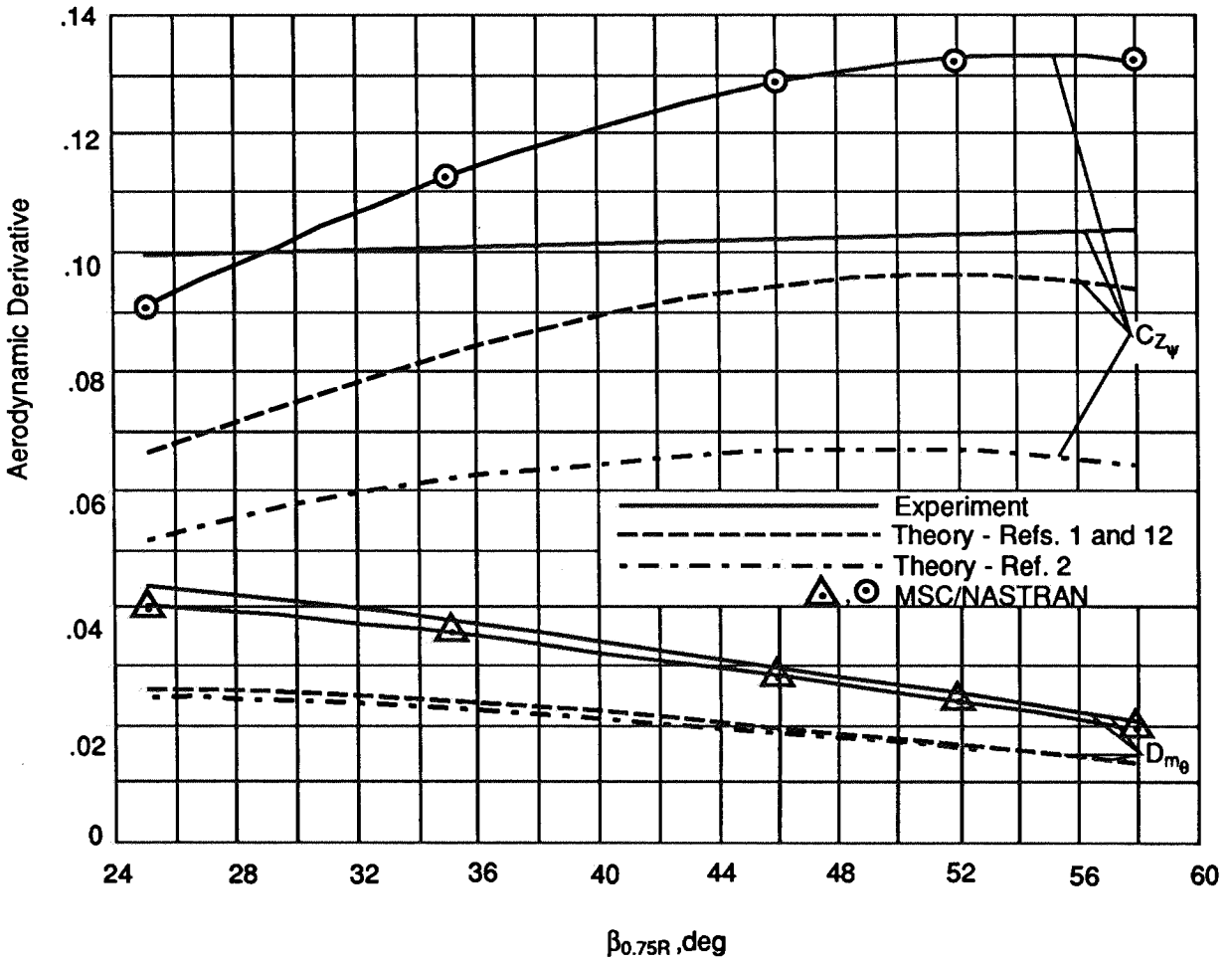

(c) C_{Z_ψ} and C_{m_θ}.

Figure 3. Comparison of Experimental and Theoretical Aerodynamic Derivatives for the Propeller of NASA TN D-1807. (Cont.)

The MSC/NASTRAN data deck requires the mechanical data for the vibration analysis and a dummy aerodynamic surface with which the propeller aerodynamics are combined in SOL 75. The abbreviated Bulk Data Deck is shown in Table 4; it is abbreviated only to the extent that a limited number of DMIG cards from the preprocessor are shown. The simple model is idealized by two grid points, the hub and the pivot, connected by a rigid bar which is connected at the pivot by pitch and yaw springs. The structural damping of the pivot springs is represented by viscous dampers using the relationship for equivalent viscous damping, e.g., $c_\theta = k_\theta g_\theta / \omega_\theta$. The concentrated mass and inertia of the propeller are located at the hub. The basic coordinate system has +x aft, +y right, and +z upward with its origin at the hub. The propeller coordinate system is the NACA system with the convention of +x forward, +y right, and +z downward.

The dummy aerodynamic surface is a flexible wing represented by three grid points, two of which are constrained and one of which is grounded by a stiff spring normal to the surface. The wing is input by CAER01, and PAER01 cards along with SPLINE2 and SET1 cards, and AERO and MKAER01 cards.

The remaining cards are required for the flutter analysis. Three vibration modes are calculated but only the two propeller/nacelle modes are used in the flutter analysis. Two FLFACT cards are used for the wing density ratio and the Mach number, and the remaining FLFACT cards list the velocities, one per card, in the analysis units that were used in the preprocessor. The FLUTTER cards, again one for each velocity, refer to the FLFACT cards and request output of both flutter solutions, one for each propeller/ nacelle mode.

The Case and Executive Control Decks are also shown in an abbreviated form in Table 4. The Executive Control Deck includes the ALTERs required to read the preprocessor data for the propeller/ nacelle. The Case Control Deck includes the SUBCASEs to perform the flutter analysis at each velocity.

The output results are shown in Figure 4. Figure 4(a) shows the variation of damping with velocity. The first propeller/nacelle mode, its backward whirl mode, goes unstable at 89 ft/s, while the second mode, the forward whirl mode, increases in stability with velocity. Figure 4(b) shows no significant variation in either frequency with velocity; the backward whirl frequency at flutter is 6.86 Hz. The experimental flutter speed was 120 ft/s with a frequency of 6.88 Hz.

Table 4. Sample Data Deck for Propeller Dynamics.

```
ID  PROP, TEST
$
$ SAMPLE AERO PROBLEM WITH PROP TERMS - NASA D-1807
$
SOL 75 $ AERO
TIME 25
$ ALTER TO ALLOW LOOPING BASED ON VELOCITY - INCLUDE PROPELLER
ALTER 830 $
$ Set counter for looping on velocity and get case control
$   for current subcase
SETVAL //V,N,REPEAT/0 $
LABEL NEWPROP $  top of velocity loop
CASE CASES,/CASES1/CEIGEN/S,N,REPEAT/S,N,LOOP/// $
$
$  alters from here until 1009 are to use new case control
$
ALTER 831,831
MTRXIN CASES1,MATPOOL,EQDYN,,TFPOOL/K2PP,M2PP,B2PP/LUSETD/S,N,
                    NOK2PP/S,N,NOM2PP/S,N,NOB2PP $
ALTER 847,847
GKAM USETD,PHIA,,LAMA,DIT,M2DD,B2DD,K2DD, CASES/ MHH,BHH,KHH,
  PHIDH/NOUE/V,Y,LMODES=0/V,Y,LFREQ=0.0/  V,Y,HFREQ=1.E30/-1/
  -1/-1/0/S,N,FMODE/V,Y,KDAMP $
ALTER 864,865
VECPLOT  PHIG,BGPDTS,EQEXINS,CSTMS,CASES1,/PHIB/0/0/1 $
SDR2 CASES1,CSTMS,MPT,DIT,EQEXINS,SILS,,,BGPDTS, LAMA,,PHIB,
            EST,/,,OPHIB,,,/C,N,REIG $
ALTER 874,874
PLOT  PLTPARA,GPSETSA,ELSETSA,CASES1,BGPA,EQAERO,SILGA,,,,/
            PLOTX4/NSILS/0/JPLOT/1/S,N,PFILE $
ALTER 907,907
SDR2 CASES1,CSTMA,MPT,DIT,EQAERO,SILA,,,BGPA,LAMA,,PHIPA,EST,/
            ,,OPHIPA,,,PPHIPA/C,N,REIG $
ALTER 910,910
PLOT  PLTPARA,GPSETSA,ELSETSA,CASES1,BGPA,EQAERO, SILGA,,PPHIPA,,/
       PLOTBX/V,N,NSILS/V,N,LUSETA/ V,N,JPLOT/-1/S,N,PFILE $
ALTER 997 $ set QHHL to 0
ADD QHHL,/QHHLNEW/(0.,0.) $
EQUIV QHHLNEW,QHHL/ALWAYS $
ALTER 998,999
FA1  KHH,BHH,MHH,QHHL,CASES1,FLIST/FSAVE,KXHH,BXHH,MXHH/
        S,N,FLOOP/S,N,TSTART/S,N,NOCEAD $
EQUIV  KXHH,PHIH/NOCEAD/BXHH,CLAMA/NOCEAD/KXHH,UHVF/NOCEAD/
        BXHH,FOL/NOCEAD/ CASES1,CASEYY/NOCEAD $
ALTER 1001,1001
CEAD     KXHH,BXHH,MXHH,EED, CASES1/PHIH,CLAMA,OCEIGS/S,N,NEIGV $
ALTER 1009  $ ALLOW LOOPING BASED ON VELOCITY
COND NOMORE,LOOP $
COND NOMORE,REPEAT $
REPT NEWPROP,50 $
LABEL NOMORE $
ENDALTER $
CEND
TITLE = PROP WHIRL SAMPLE - PROP FROM NASA D-1807 - data from PROP
SUBT = User-supplied Aspect ratio
LABEL = PK METHOD FLUTTER SOLUTION - NO DMIG ON SUB 1
SEALL=ALL
SPC   = 1
$
```

Table 4. Sample Data Deck for Propeller Dynamics. (Cont.)

```
$ Only two subcases are shown...one is needed for each velocity
$
SUBCASE 1
LABEL = SUBCASE 1 - FMETHOD = 30 - VELOCITY = 1 FT/SEC
METHOD  = 10
FMETHOD = 30
$ B2PP=AEROB101
$ K2PP=AEROS101
SUBCASE 2
LABEL = SUBCASE 2 - FMETHOD = 40 - VELOCITY = 10 FT/SEC
METHOD  = 10
FMETHOD = 40
 B2PP=AEROB102
 K2PP=AEROS102
$
$  additional subcases
$
BEGIN BULK
$
$  PROP GRID IS 999 - ATTACHED TO GRID 1000 BY CELAS FOR FREQUENCIES
$
GRID    999             .0      0.000   .0      15
RBAR    1000    999     1000            123456
GRID    1000            3.5035  0.0     .0              1234
$ coordinate system for prop points - pointing -x and -z
CORD2R  15              0.      0.      0.      0.      0.      -1.     +cr15
+cr15   -1.     0.      0.
$
$ CONCENTRATED MASS FOR PROP
$
CONM2   999     999             3.82711                                 +PROP
+PROP                   246.761                 246.761
$
PARAM   WTMASS  .0025901
$
$ CELAS2 ELEMENTS TO OBTAIN FREQUENCIES
$
CELAS2  1       2542.2  1000    5
CELAS2  2       2498.2  1000    6
EIGR    10      GIV     .0      30.             3                       +ER
+ER     MAX
$ SET DENSITY
FLFACT  1       0.8873                                                  DENS
FLFACT  2       0.10                                                    MACH
$ ONE VELOCITY PER SUBCASE
FLFACT  3       1.0                                                     VELOC
FLFACT  4       120.                                                    VELOC
FLFACT  5       240.                                                    VELOC
FLFACT  6       360.                                                    VELOC
FLFACT  7       480.                                                    VELOC
FLFACT  8       600.                                                    VELOC
FLFACT  9       720.                                                    VELOC
FLFACT  10      840.                                                    VELOC
FLFACT  11      -960.                                                   VELOC
FLFACT  12      -1080.                                                  VELOC
FLFACT  13      1200.                                                   VELOC
FLFACT  14      1320.                                                   VELOC
```

Table 4. Sample Data Deck for Propeller Dynamics. (Cont.)

```
$ set up flutter cases
FLUTTER 30      PK      1       2       3       L       2
FLUTTER 40      PK      1       2       4       L       2
FLUTTER 50      PK      1       2       5       L       2
FLUTTER 60      PK      1       2       6       L       2
FLUTTER 70      PK      1       2       7       L       2
FLUTTER 80      PK      1       2       8       L       2
FLUTTER 90      PK      1       2       9       L       2
FLUTTER 100     PK      1       2       10      L       2
FLUTTER 110     PK      1       2       11      L       2
FLUTTER 120     PK      1       2       12      L       2
FLUTTER 130     PK      1       2       13      L       2
FLUTTER 140     PK      1       2       14      L       2
PARAM   LMODES  3
PARAM   VREF    12.0
$
$ AERO CARD FOR REF CHORD = 4.375
$
AERO                    4.375   1.1468-7
$
CAERO1  2000    2000            2       2                       1       +CAC
+CAC    0.      0.      0.      1.0     0.      1.0     0.      1.0
PAERO1  2000
MKAERO1 0.0                                                             +MK
+MK     .001
GRID    1001            0.0     0.0     0.0             123456
GRID    1002            1.0     0.0     0.0             123456
GRID    1003            0.0     1.0     0.0             12456
CELAS2  1004    1.0+6   1003    3
CONM2   1004    1003            1.0
SPLINE2 2000    2000    2000    2003    2000    0.      1.              +SPC
+SPC    -1.     -1.
SET1    2000    1001    1002    1003
$
$  damping elements
$
CDAMP1,101,101,999,5
CDAMP1,102,102,999,6
PDAMP,101,.26387,102,.39237
$
$  DMIG cards created by PROP using input from D1807A.DAT
$
$
$ RESULTS FROM PROGRAM PROP FOR THE FOLLOWING PROBLEM
$ D-1807 - run 1 - omega=2304 - A=3.47
$ THE FOLLOWING MATRICES (AEROS101 AND AEROB101) ARE BASED ON
$  VELOCITY =  1.000000E-01(ft/sec)
$  MACH NO  =  8.960574E-05
$  DENSITY  =  1.017600E-07
DMIG    AEROS101        0       1       1
$
$  DMIG ENTRIES CREATED BY PRE-PROCESSOR
$
*D100490              999               6 6.669288278E-01                *D100491
ENDDATA
```

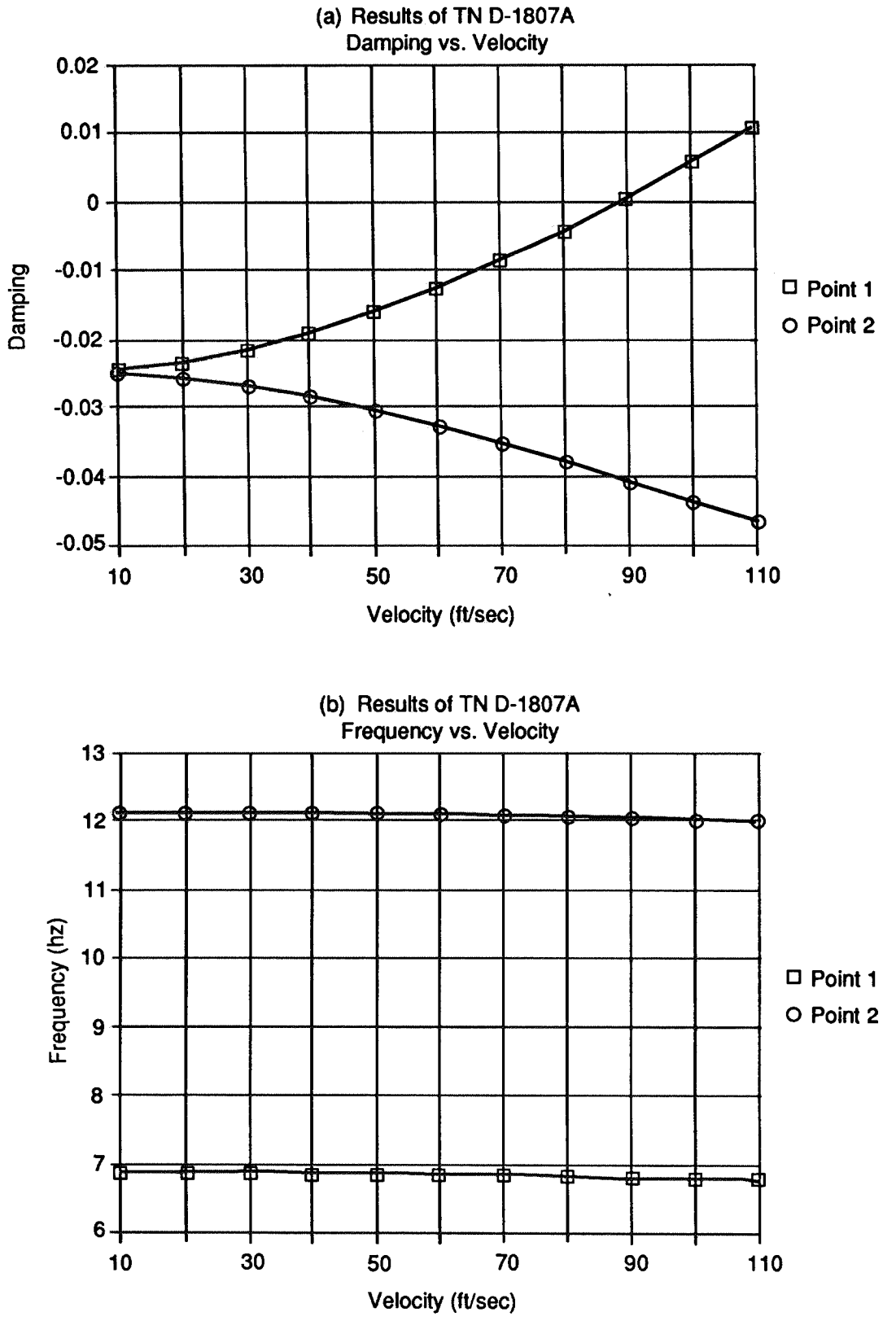

Figure 4. Damping (a) and Frequency (b) vs. Velocity for Example TN D-1807A.

Additional flutter cases in Reference 5 were analyzed and the results are summarized in Table 5. The cases selected from Table 2 of Reference 5 may be characterized by their blade reference angles $\beta_{0.75R}$ and uncoupled pitch frequencies f_θ. Table 5 presents the experimental and calculated flutter speeds and frequencies; the subscripts e and c denote experimental and calculated values, respectively. The results from the example problem are also shown for completeness.

Table 5. Comparison of Some Experimental and Calculated Flutter Speeds and Frequencies.

$\beta_{0.75R}$	f_θ (Hz)	V_e (ft/s)	f_e (Hz)	V_c (ft/s)	f_c (Hz)	V_c/V_e
35	9.20	120	6.88	89	6.86	0.742
35	10.96	159	7.58	130	7.88	0.818
46	10.96	167	8.30	137	8.57	0.820
52	10.96	186	8.63	144	8.77	0.774
58	10.96	210	8.75	152	8.96	0.724
58	10.71	231	8.10	176	8.18	0.762

A perusal of Table 5 indicates that the aerodynamic theory of Reference 2, as implemented in MSC/NASTRAN, is reasonably conservative in predicting flutter speeds and reasonably accurate in predicting flutter frequencies. This conservatism in flutter speed is in agreement with the results shown in Figure 16 of Reference 5.

BAH Wing/Nacelle with Propeller/Rotor

This example is the BAH wing, i.e., the wing studied throughout Reference 13, modified to have a nacelle. The model for this problem is based on Example HA75B in the MSC/NASTRAN Handbook for Aeroelastic Analysis. The nacelle is added at the engine station at Wing Station (WS) 186.0 as shown in Figure 5. The propeller is assumed to have four blades, a diameter of 7.0 ft., and to weigh 400 lbs. The nacelle is assumed to be 36.0 in. in diameter and to extend 100.0 in. forward of the wing leading edge at WS186.0. The aerodynamic data are changed to obtain the wing nacelle interference effects; the wing mass data for the section at WS186.0 are adjusted to account for the assumed propeller weight of 400 lbs. while maintaining the original inertial characteristics of the section, i.e., total weight, centroid, and pitching moment of inertia.

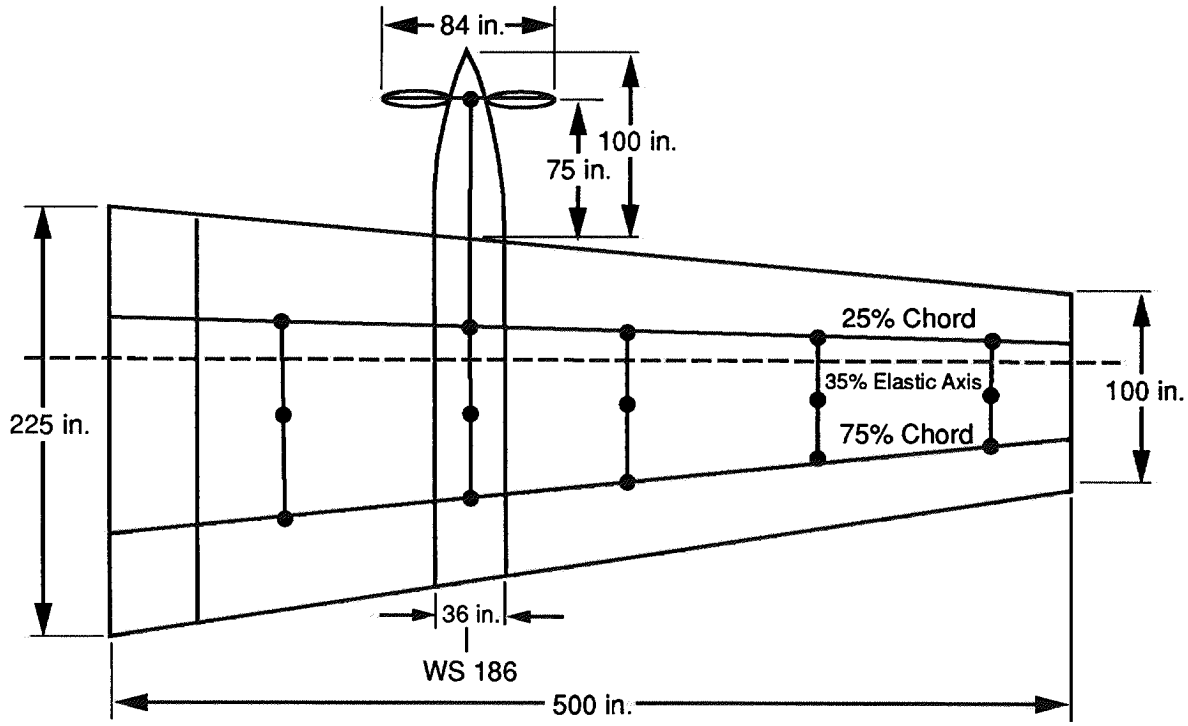

Figure 5. BAH Wing with Nacelle and Propeller.

The addition of the nacelle to Example HA75B requires modifying the CAER01 and PAER01 cards and adding CAER02 and PAER02 cards. Two CAER01 cards are now needed for the wing inboard and outboard of the nacelle. The first CAER01 card divides the inboard wing into 12 boxes from the centerline to WS168.0, and the second CAER01 card divides the outboard wing into 16 boxes from WS204.0 to the tip at WS500.0. Linear splines, SPLINE2 cards, connect the inboard and outboard wings to all of the wing grid points. The PAER01 card refers to the CAER02 card which defines the 278.5 in. long nacelle. An AEFACT card divides the nacelle into six slender body elements with six interference elements. The forward slender body element of the nacelle represents the propeller "spinner" and is 50.0 in. long; the forward element must be centered at the propeller hub since the wing flow field effects at the propeller hub are determined by the flow around the interference element circumscribing the forward slender body element. Only the interference from the wing downwash is considered in this example (i.e., sidewash is neglected) so the PAER02 card prescribes vertical motion only (a z-body) and, on another AEFACT card, the interference flow field is only sampled at the top ($\theta = 90^\circ$) and bottom ($\theta = 270^\circ$) of the nacelle on its centerline.

The forward nacelle structure is assumed to consist of a rigid element (RBAR) connecting the hub to a pivot at the forward wing grid point at WS186.0. The RBAR is supported by the wing via pitch and yaw springs (CELAS4); the yaw spring is assumed to be 25% stiffer than the pitch spring. The nacelle linear spline connects the nacelle to the three grid points at WS186.0: the fore and aft points on the wing, and the point at the propeller hub. The flutter solution, SOL 75, requires the aerodynamic coordinate system to have +x in the streamwise direction, whereas the propeller aerodynamics are developed in the

standard NACA stability axis system with +x forward. Two coordinate systems (CORD2R) are therefore used, the first defining the aerodynamic coordinate system, and the second defining the propeller system.

The data for the propeller/nacelle aerodynamic and gyroscopic loads begin with the propeller geometry. A blade is assumed to have a constant chord of 17.50 in beyond the dimensionless radius of $\eta_o = 0.27$; the reference chord is $c_r = 17.50$ in. and the radius is R = 42.00 in., and there are four blades. The flutter solution of Example HA75B assumed incompressible aerodynamics on the wing; for consistency with that solution, the speed of sound in the propeller/nacelle preprocessor is set to 10^6 fps, and no significant compressibility correction appears in the blade aerodynamic coefficient calculation. The gyroscopic effects are determined by the propeller polar moment of inertia, assumed to be $I_x = 6000$ lb-ft^2, the rotor polar moment of inertia, assumed to be, $I_r = 60$ lb-ft^2, and the assumed gear ratio $N_r = 12$; the propeller is assumed to be rotating at 2000 RPM. The flutter analyses are performed at sea level with an air density of $\rho = 0.002378$ slug/cu. ft.

The Bulk Data Cards for the flutter solution are the same as in Example HA75B (with additions and modifications noted above) except that multiple FLFACT and FLUTTER cards are required for each case (each combination of density, velocity and speed of sound) in the preprocessor. All structural damping is neglected, both in the wing and in the engine mounts. The Case and Executive Control Decks are similar to those shown in Table 4 for the previous example.

A number of studies have been made on this configuration. First, the aerodynamic effects of the nacelle with no rotation have been investigated. Two cases are considered: the rigid and the flexible nacelle. The flutter and divergence speeds are shown in Table 6 and compared with Example HA75B.

Table 6. The Effects of the Nacelle on the Flutter and Divergence Speeds of the BAH Wing.

Configuration	V_f (ft/s)	V_d (ft/s)
No Nacelle (HA75B)	1056	1651
Rigid Nacelle	1065	1635
Flexible Nacelle	1118	1608

The aerodynamic effect of the nacelle is a reduced loading in the nacelle region accompanied by a forward movement of the aerodynamic center. In the case of the rigid nacelle, the net effect is a slight increase in flutter speed and a slight decrease in divergence speed. With flexibility added, the modified nacelle aerodynamic loading results in a further increase in flutter speed and further decrease in divergence speed. The damping and frequency curves are shown in Figure 6 for the case of the flexible nacelle; they are similar to the curves for Example HA75B in Figure 5 of Section 6.2.2 of the MSC/NASTRAN Handbook for Aeroelastic Analysis.

The second study is the effect of rotational speed on the vibration frequencies. The results are presented in Table 7 for the rigid and flexible nacelles with various rotational speeds: the second column gives the frequencies (Hz) for the rigid nacelle without rotation; the remaining columns give the frequencies for the flexible nacelle with the rotational speeds (RPM) indicated.

Table 7. Effect of Propeller Rotational Speed on Vibration Frequencies of the BAH Wing.

	Rigid Nacelle	Flexible Nacelle		
Mode	$\Omega = 0$	$\Omega = 0$	$\Omega = 1000$	$\Omega = 2000$
1	2.037	2.037	2.037	2.036
2	3.553	3.466	3.389	3.129
3	7.280	5.861	5.012	4.428
4	11.699	6.174	7.103	7.240
5	14.881	7.355	7.642	9.162

The rigid nacelle frequencies are the same as Example HA75B and provide a check on the modified mass matrix. The flexible nacelle has its pitch and yaw frequencies between the wing second and third frequencies: the pitch frequency is 5.861 Hz and the yaw frequency is 6.174 Hz. The effect of the gyroscopic moments is to decrease the lower frequencies and increase the higher frequencies.

The final study is the whirl flutter characteristics of the wing/engine system. Two cases are considered: first without and then with the interference from the wing downwash field. The damping and frequency curves without the wing downwash are presented in Figure 7; the curves with the downwash are shown in Figure 8. The flutter and divergence speeds are summarized in Table 8. In comparing Figures 6 and 7 or 8, it is noted that the wing torsion mode (Point 2) has been stabilized by the propeller effects. As expected, in Figures 7 and 8, the backward whirl mode (Point 3) goes unstable while the forward whirl mode (Point 4) remains stable. In comparing Figures 7 and 8, the flow field effects are seen to be stabilizing on the flutter speed, whereas they are destabilizing on the divergence speed, also as expected.

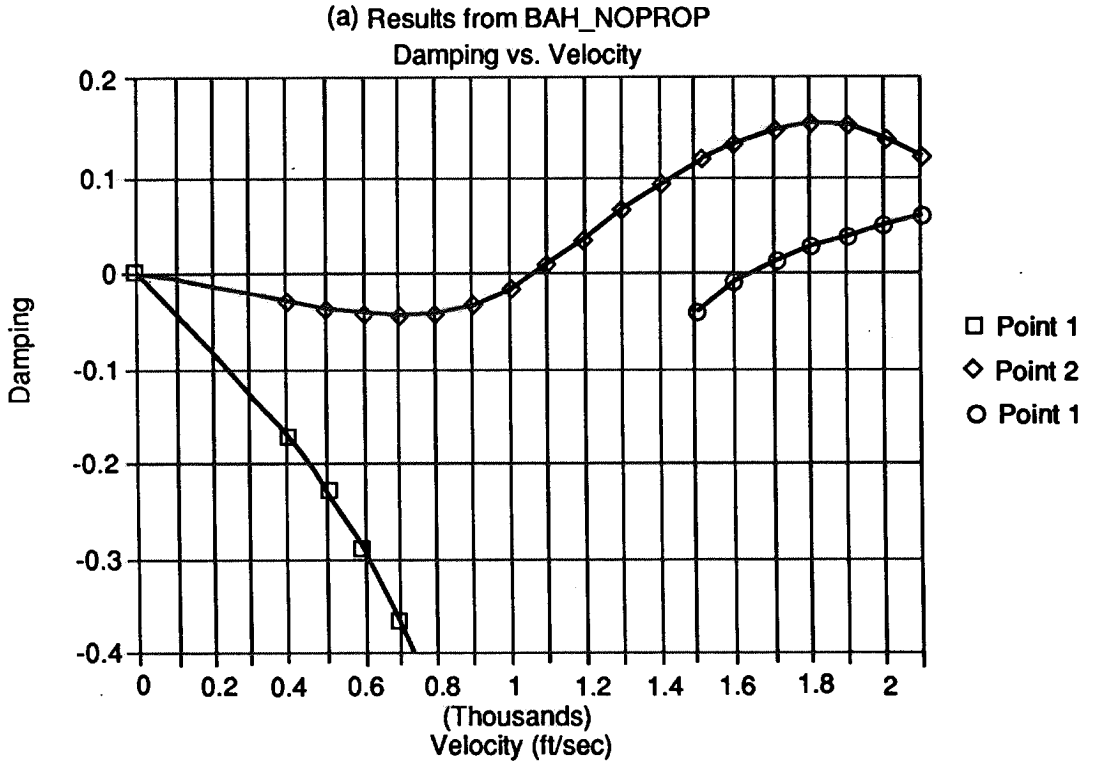

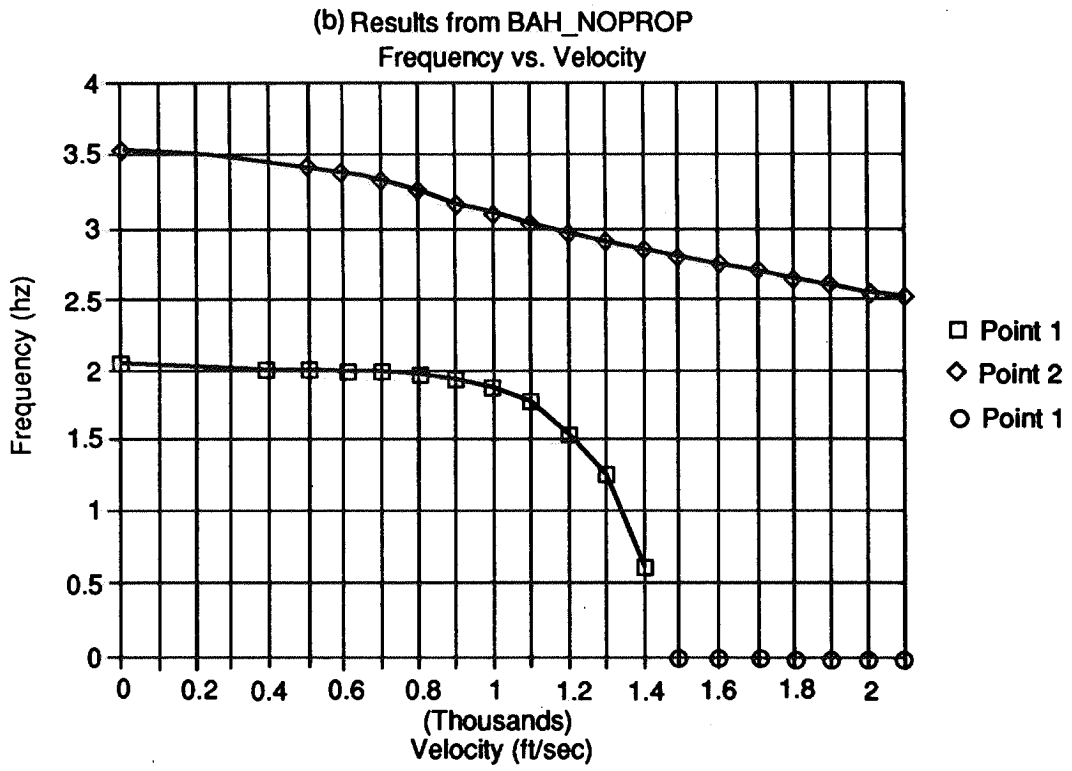

Figure 6. Damping (a) and Frequency (b) vs. Velocity for BAH Wing with Flexible Nacelle.

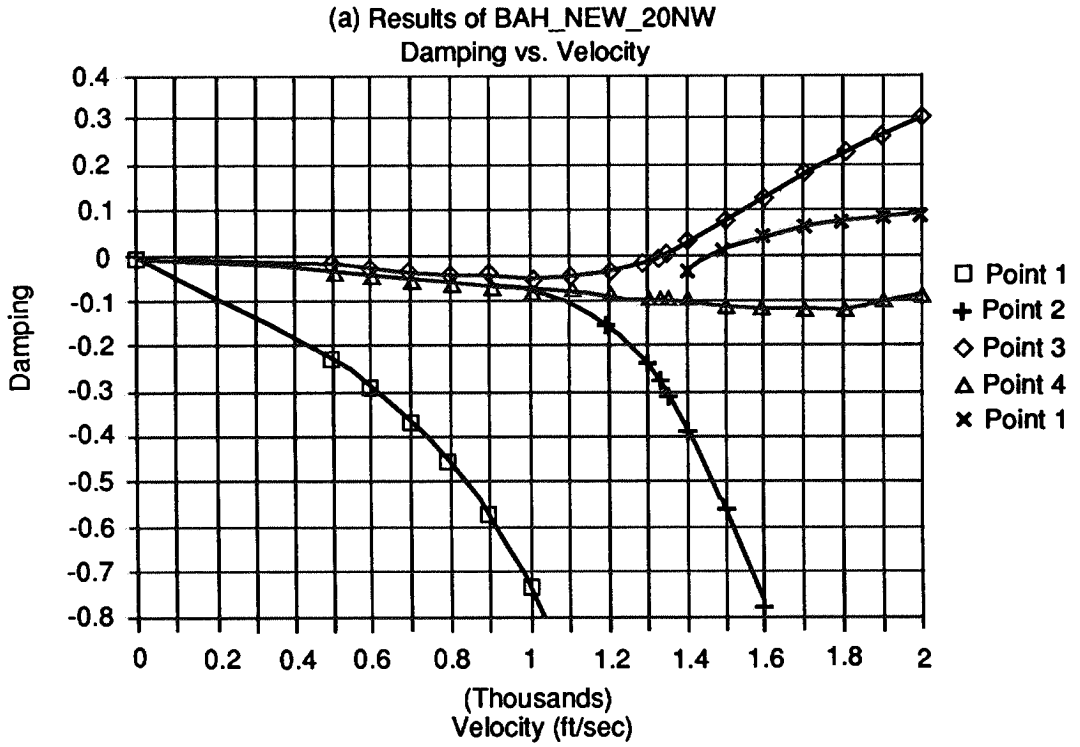

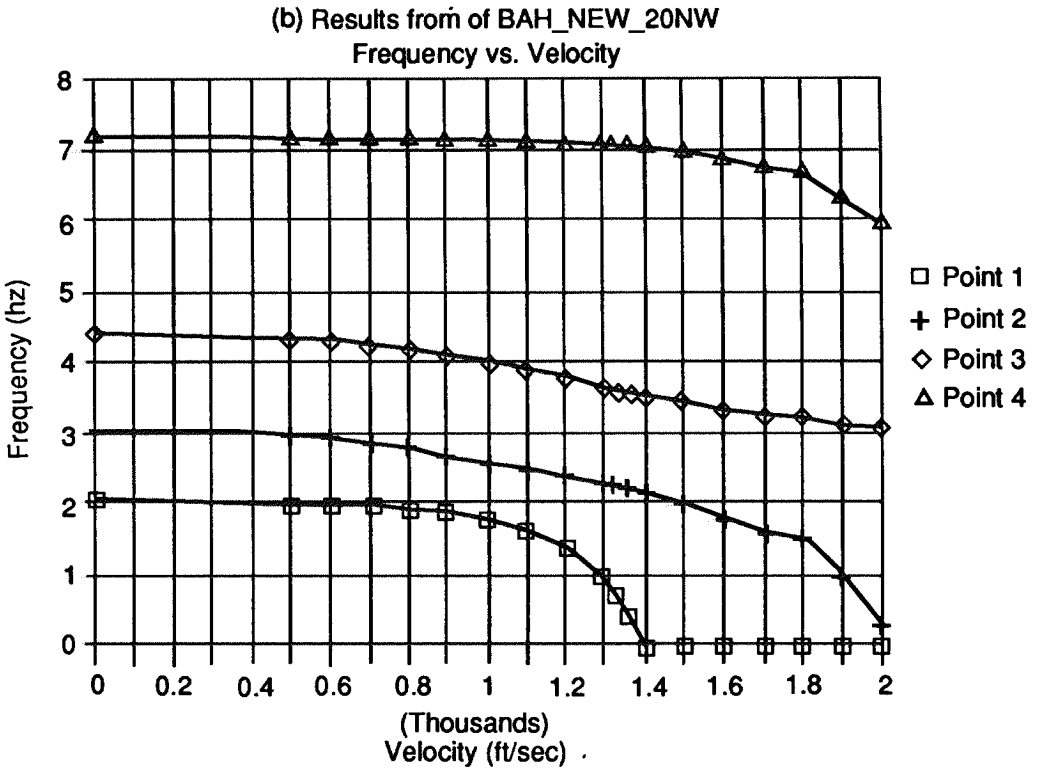

Figure 7. Damping (a) and Frequency (b) vs. Velocity for BAH Wing/Nacelle/Propeller Without Wing Downwash.

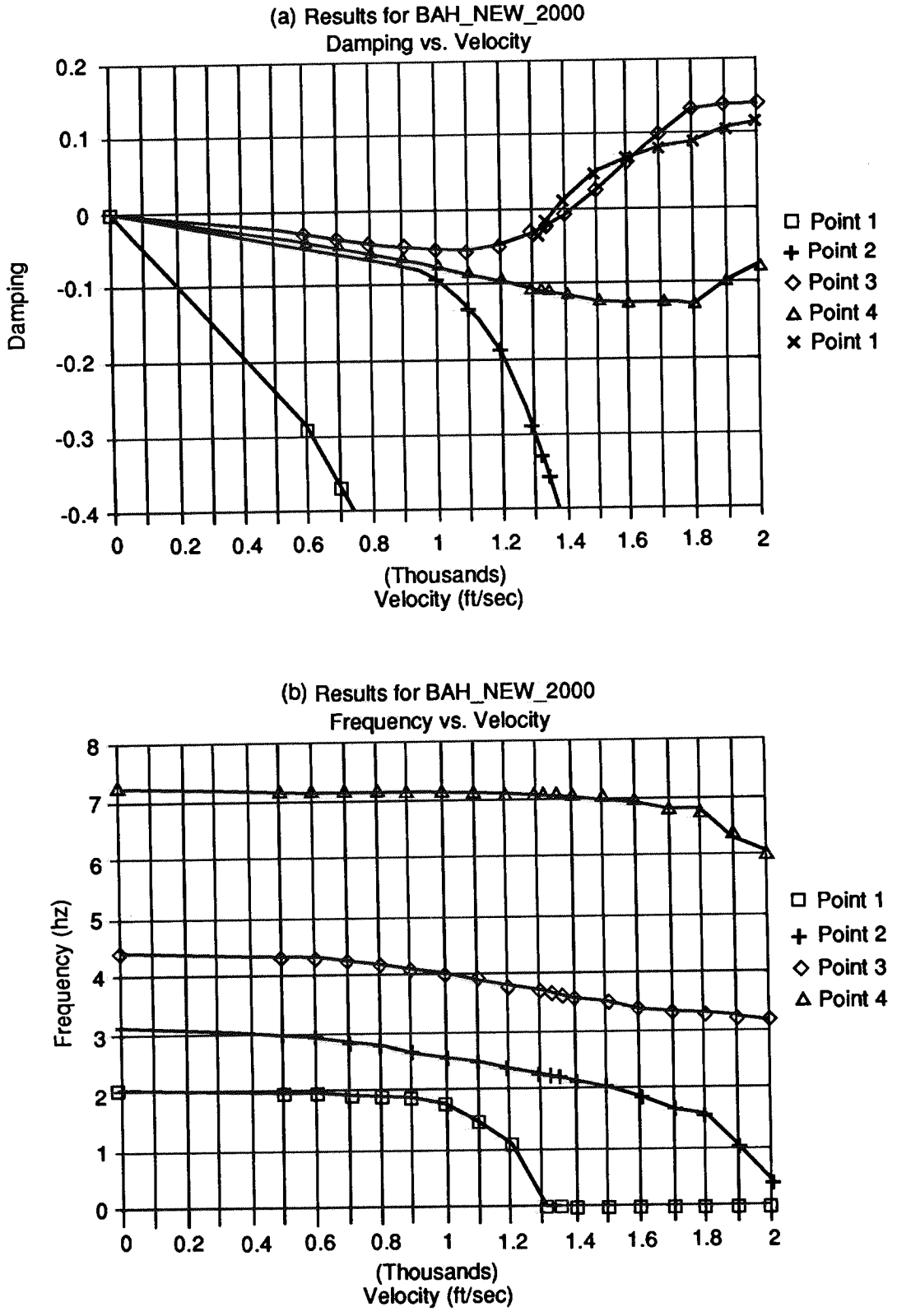

Figure 8. Damping (a) and Frequency (b) vs. Velocity for BAH Wing/Nacelle/Propeller With Wing Downwash.

Table 8. Effect of Wing Downwash on the Flutter and Divergence Speeds of the BAH Wing/Engine.

Downwash	V_f	V_d
no	1350	1467
yes	1423	1372

Correction Factors to Account for the In Propeller Slipstream

Simple momentum theory for propellers can be utilized to determine the slipstream velocity in the wake of a propeller as well as its width. Any textbook on helicopters suggests the following analysis. Figure 9 illustrates the geometry and velocities.

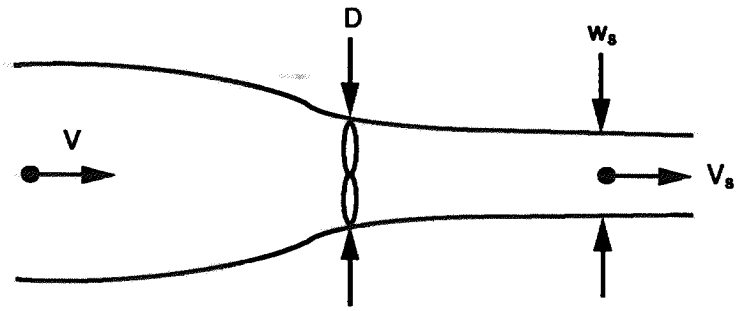

Figure 9. Geometry and Velocities Around Propeller.

The momentum equation gives the thrust

$$T = S_s \rho V_s (V_s - V) \tag{37}$$

where S_s is the cross section area of the slipstream, and the energy equation also gives the thrust

$$T = \frac{1}{2} S\rho\left(V_s^2 - V^2\right) \tag{38}$$

From the energy equation the slipstream velocity is found

$$V_s = V\sqrt{1 + 2T/\rho V^2 S} \tag{39}$$

By combining the momentum and energy equations, the slipstream area is found

$$S_s/S = \frac{1}{2}\left(1 + 1/\sqrt{1 + 2T/\rho V^2 S}\right) \tag{40}$$

and its width is

$$w_s = (4/\pi)\sqrt{S_s} \tag{41a}$$

$$= (D/\sqrt{2})\left(1 + 1/\sqrt{1 + 2T/\rho V^2 S}\right)^{\frac{1}{2}} \tag{41b}$$

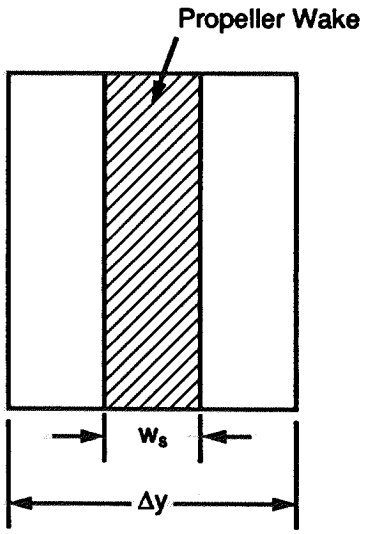

Figure 10. Geometry for Correction Factors.

The correction factor is derived from the slipstream velocity and width with the aid of the geometry in Figure 10. The lift effectiveness in the stripstream is increased by the factor $(V_s/V)^2$, and the correction factor measures the average lift on the wing boxes and slender body elements in the region of the propeller wake. If the wing/body region to be adjusted has width Δy, then the correction factor is assumed to be

$$W_{kk} = [\Delta y - w_s + (V_s/V)^2 w_s]/\Delta y \tag{42a}$$

$$= 1 + (D/\Delta y)\left(1 + 1/\sqrt{1 + 2T/\rho V^2 S}\right)^{\frac{1}{2}}(\sqrt{2}\,T/\rho V^2 S) \tag{42b}$$

This correction factor is not illustrated in the above example of the BAH wing/nacelle since engine thrust estimates are not available for the airplane. However, the correction factors would be included in the data deck as illustrated in various examples in the MSC/NASTRAN Handbook for Aeroelastic Analysis: the DMI cards in the Bulk Data Deck, and the ALTER in the Executive Control Deck (Note: the ALTER is required in V65).

CONCLUDING REMARKS

A new capability for flutter analysis in MSC/NASTRAN has been developed in a preprocessor to SOL 75 to account for propeller/nacelle aerodynamic and gyroscopic loads. The effects of the wing downwash and sidewash the propeller loads have been considered, and the effect of the propeller wake on the wing has also been considered. The primary effects of the propeller/nacelle combination have been demonstrated in two examples with some experimental correlation.

ACKNOWLEDGMENT

The authors wish to acknowledge Samuel G. Westwood of the Greenville Division of E-Systems, Inc., for partial support of this development.

REFERENCES

1. Reed, Wilmer H., III, and Bland, Samuel R., "An Analytical Treatment of Aircraft Propeller Precession Instability," NASA TN D-659, January 1961.

2. Houbolt, John C., and Reed, Wilmer H., III, "Propeller-Nacelle Whirl Flutter," J. Aero. Sci., March 1962, pp. 333-346.

3. Sewell, John L., "An Analytical Trend Study of Propeller Whirl Instability," NASA TN D-996, April 1962.

4. Abbott, Frank T., Jr., Kelly, H., Neale, and Hampton, Kenneth D., "Investigation of Propeller-Power-plant Autoprecession Boundaries for a Dynamic-Aeroelastic Model of a Four-Engine Turboprop Transport Airplane," NASA TN D-1806, August 1963.

5. Bland, Samuel R., and Bennett, Robert M., "Wind-Tunnel Measurement of Propeller Whirl-Flutter Speeds and Static Stability Derivatives and Comparison with Theory," NASA TN D-1807, August 1963.

6. Bennett, Robert M., and Bland, Samuel R., "Experimental and Analytical Investigation of Propeller Whirl Flutter of a Power-plant on a Flexible Wing," NASA TN D-2399, August 1964.

7. Smith, G. E., "Whirl of an Aircraft Power-plant Installation and its Interaction with the Flutter Motion of a Flexible Wing," British A.R.C. R. & M. No. 3536, August 1966.

8. Reed, Wilmer H., III, "Review of Propeller-Rotor Whirl Flutter," NASA TR R-264, July 1967.

9. Kvaternik, Raymond G., "Studies in Tilt-Rotor VTOL Aircraft Aeroelasticity," Ph.D. Dissertation, Case Western Reserve University, Cleveland, Ohio, June 1973.

10. Förstching, Hans W., Grundlagen der Aeroelastik, Berlin: Springer-Verlag, 1974.

11. Kvaternik, Raymond G., and Kohn, Jerome S., "An Experimental and Analytical Investigation of Proprotor Whirl Flutter," NASA Technical Paper 1047, December 1977.

12. Ribner, Herbert S., "Propellers in Yaw," NASA Report No. 820, 1945.

13. Bisplinghoff, R.L, Ashley, H., and Halfman, R.L., Aeroelasticity, Reading: Addison-Wesley Publishing Co., 1955.